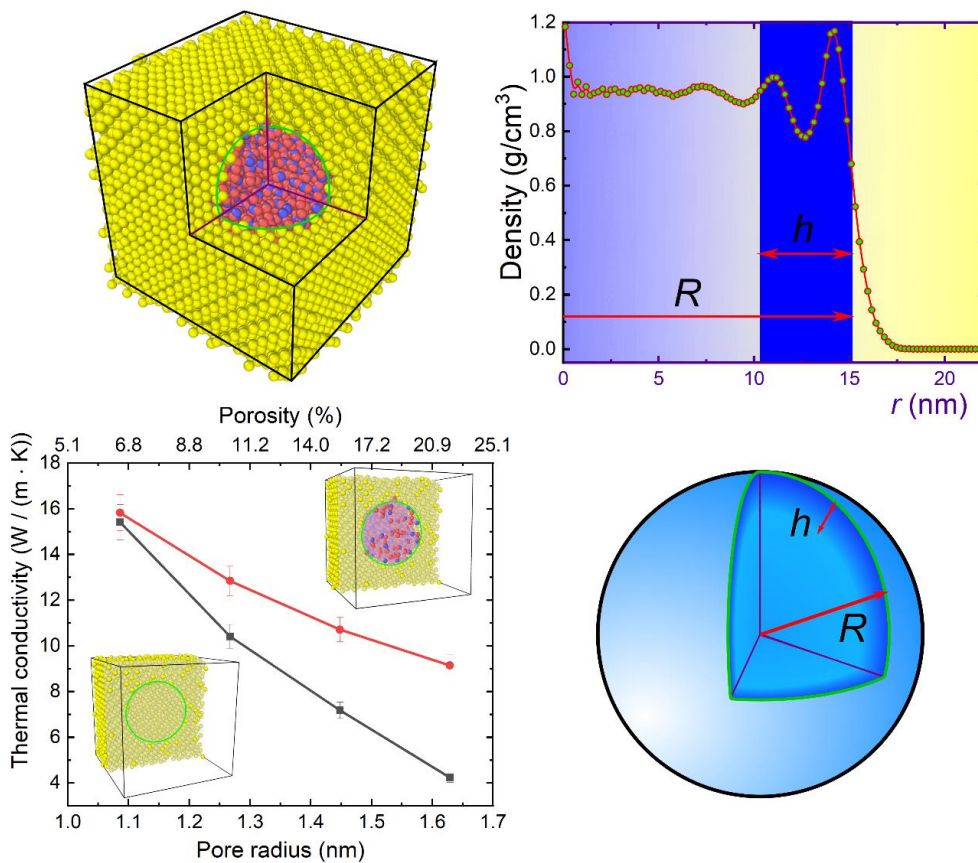# Thermal transport enhancement due to confined water in hybrid nanocomposite

Mykola Isaiev[1*], Xiaorui Wang[2], Konstantinos Termentzidis[2], and David Lacroix[1]

[1]*Université de Lorraine, CNRS, LEMTA, Nancy F-54000, France*

[2]*Univ Lyon, INSA-Lyon, CETHIL CNRS-UMR5008, F-69621, Villeurbanne, France*

Corresponding author: mykola.isaiev@univ-lorraine.fr

Abstract

The thermal transport properties of porous silicon and nano-hybrid "porous silicon/water" systems are presented here. The thermal conductivity was evaluated with equilibrium molecular dynamics technique for porous systems made of spherical voids or water-filled cavities. We revealed large thermal conductivity enhancement in the nano-hybrid systems as compared to their dry porous counterparts, which cannot be captured by effective media theory. This rise of thermal conductivity is related to the increases of the specific surface of the liquid/solid interface. We demonstrated that significant difference for more than two folds of thermal conductivity of pristine porous silicon and "porous silicon liquid – composite" is due to the liquid density fluctuation close to "solid-liquid interface" (layering effect). This effect is getting more important for the high specific surface of the interfacial area. Specifically, the enhancement of the effective thermal conductivity is 50 % for specific surface area of 0.3 (1/nm), and it increases further upon the increase of the surface to volume ratio. Our study provides valuable insights into the thermal properties of hybrid liquid/solid nanocomposites and about the importance of confined liquids within nanoporous materials.

Manipulation of heat flux at different scales is one of the key factors for improving reliability and lifetime of different devices (electronics, optics, spintronic, etc.). Specifically, efficient thermal management gives the possibility to overcome the occurrence of "hot-spots" in the semiconductor's materials[1], which are the base components of nano-electronics. Therefore, tuning the thermal conductivity (TC) of materials through nano-structuration, as well as, understanding heat transport in those compounds is crucial for tomorrow practical applications, e.g. 5nm MOFSET technology[2].

From this point of view, nano-hybrids systems like the nanofluids, are well known media that improve heat transport. For instance, one can achieve important enhancement of thermal conductivity of a liquid by adding inside only a small amount of nanoparticles[3]. Such phenomena arise mainly because of significant surface to volume ratio of nanoparticles incorporated in the fluid[4]. The latter mechanism makes nanofluids promising candidates in various cooling applications[5,6]. Nevertheless, nanofluids are liquids, and they are often incompatible with electronic solid-state technologies.

Another important family of materials with significant interfacial area is nanoporous materials. From both experimental[7,8] and theoretical point[9–12] of view, it is well-known that such materials demonstrate significant reduction of thermal conductivity compared to the bulk ones. The main mechanism of the TC reduction in nanoporous materials is related to the phonon scattering on the pore edges. Thus, the porous matrix filled by a liquid agent may demonstrate similar behavior as nanofluids. Particularly, significant rise of thermal conductivity of porous silicon-liquid composite system while compared to the pristine ones was already observed experimentally[13,14]. However, the nature of heat transport is significantly different for nanofluids and for nano-hybrids systems based on porous materials compared to nanofluids. In the latter case a substantial part of the thermal energy is transferred through the solid matrix[15]. In crystalline matrix (like for the porous silicon), one should consider phonon contribution to heat transfer, with associated sub-issues like scattering phenomena at the interfaces involving interfacial boundary resistance[16,17] and the presence of the adsorbed liquid layer close to the interface[18]. Moreover, strong

2

confinement substantially modifies properties of water[19]. The above-mentioned issues are key points to control heat transfer by using hybrid-like porous composites in nanoscale devices. The understanding of thermal transport mechanisms in nanoporous crystalline matrix-liquid composite is in the core of this article; investigations are carried out using atomistic molecular dynamics (MD) approach.

Ming Hu et al[20] have already reported a significant increase and a nonmonotonic dependence of the overall interfacial thermal conductance between quartz and water layer due to the freezing of water molecules at extremely confined conditions and the vibrational states match between trapped water and the solid. The behaviour of water molecules within nanopores with crystalline pore walls has been examined by Watanabe[21] and it has been found to be very sensitive to the pore structure (shape of the pore section and periodicity) and to the degree of pore filling with water.

In our study the matrix is crystalline silicon with diamond-type lattice. The lattice parameter (a_0) equals to 5.43 Å. Equilibrium Molecular Dynamic (EMD) simulations of solid phase are performed using the Stilling-Weber[22] interatomic potential. We considered nano-porous silicon (np-Si) systems with porosity in the range 3% < P < 28%. Concerning nanohybrid (nh) configurations, they are like the dry ones but now the voids are filled with water molecules. The number of water molecules was chosen to reach the averaged density inside pore approximately equals to 1 g/cm³. The SPC/E water model[23] is used for modelling the interactions between water atoms. The interaction forces between oxygen atoms and silicon atoms are treated with the Lenard-Jones potential. Potential parametrization is taken from a previous study[24]. In this framework we neglect the interactions between hydrogen and silicon atoms. Two sizes of simulation box are considered with length of $8a_0 \times 8a_0 \times 8a_0$ and $10a_0 \times 10a_0 \times 10a_0$. Eventually, periodic boundary conditions are used in all directions. All simulations were carried with the use of Large-scale Atomic/Molecular Massively Parallel Simulator (LAMMPS)[25].

For thermal conductivity evaluations the equilibrium molecular dynamics (EMD) approach, which is based on the Green-Kubo equation for autocorrelations of heat flux, is used:

$$\kappa_{\alpha\beta} = \frac{1}{Vk_bT^2}\int\limits_0^\infty dt\langle J_\alpha(t)\cdot J_\beta(0)\rangle, \qquad (1)$$

where V is the system volume, k_b is the Boltzmann constant, T is the system temperature, $J_\alpha(t)$ is the heat flux in direction α at time step t.

Before calculations of heat flux correlations, the systems were equilibrated according to Nose-Hoover thermostat during 2 ns with the use of canonical (NVT) ensemble. Snapshots of equilibrated systems for the two box sizes with different pore radii are presented in insets of Fig. 1. After equilibrium, we performed NVE integration during 20 ns. During this integration the heat flux in each direction was recorded. The correlation time length was set to 2 ps, and the sampling interval was 40 ps.

First, the thermal conductivity (κ) of a bulk water sample was simulated to test the reliability of our EMD modelling with SPC/E potential. In the present work, the thermal conductivity of pure water was found to be equal to 0.86 W/(m K). This value is higher than the experimental one (0.591-0.607 W/(m K)), but it matches well with other molecular dynamics studies[26] for the same water model.

The thermal transport properties of several np-Si and nh systems with spherical pores are investigated. The thermal conductivities of pristine and nanohybrid systems are presented in the Fig. 1 as a function of pore radius (lower-axis) and porosity (upper-axis) for two sizes of simulation domain. As expected, a strong reduction of (κ) is observed in dry nanoporous samples as porosity increases. Additionally, Fig. 1a clearly shows significant enhancement of thermal conductivity of nh system as compared to the pristine ones for the simulation domain sizes equal to $8a_0 \times 8a_0 \times 8a_0$. The thermal conductivity enhancement continuously increases with the pore radius, and it even double for the biggest considered radius ($R = 3a_0$ = 1.63 nm), showing that the presence of water molecules within the pore strongly contribute to heat transport. Fig. 1b depicts the results when the simulation domain has length size equals to 10a. Logically, both dry and wet systems leads to smaller TC values while the pore radius increases and nh systems exhibit almost systematically larger κ than np-Si. More interestingly, the relative increase of nh thermal conductivity is less pronounced even for the same porosities as those computed for the 8a×8a×8a box size (e.g. the penultimate point in Fig. 1b and the last one in Fig. 1a). Since the porosity is a volumetric characteristic parameter, one can conclude that the TC enhancement between dry and wet systems has a nanoscale nature where surface phenomena dominate. This issue is further investigated in order to determine the relevant parameters that rule heat transport.
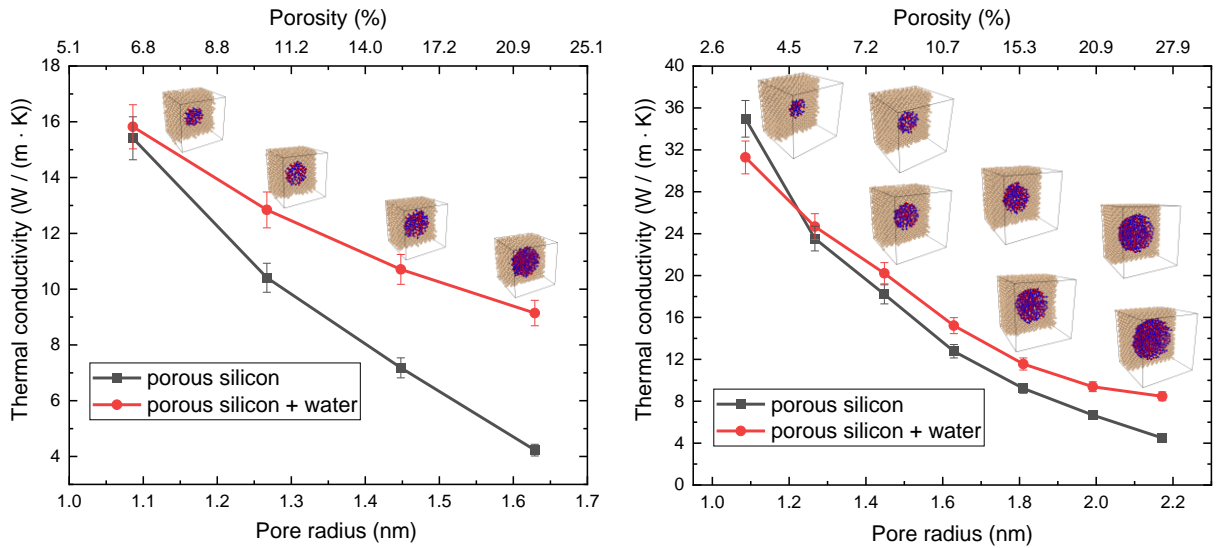

Figure 1. Dependence of thermal conductivity on the pore radius (lower axis) and porosity (upper) axis for the two domains' sizes: 8a_0×8a_0×8a_0 (a) and 10a_0×10a_0×10a_0 (b). The black points correspond to the dry samples, while the red ones to the wet samples. The lines are guide to eyes. The insets show MD snapshots for corresponding pore' radius (porosity)

According to Nan et al [27] effective medium theory, thermal conductivity of a composite can be modelled as follows:

$$\kappa_{comp} = \kappa_m \times F, \tag{2}$$

where κ_m is the thermal conductivity of the matrix, F is the factor which describes the effect of material constitution. A simple description of the volumetric factor can be taken from two phase Maxwell effective model [28], it reads:

$$F = \frac{\kappa_f(1 + 2\alpha) + 2\kappa_m + 2P\big(\kappa_f(1 - \alpha) - \kappa_m\big)}{\kappa_f(1 + 2\alpha) + 2\kappa_m - P\big(\kappa_f(1 - \alpha) - \kappa_m\big)}, \tag{3}$$

where κ_f is the thermal conductivity of the filler (fluid in our case), κ_m is the thermal conductivity of matrix, P is the porosity, $\alpha = \delta/R$ is the dimensionless parameter which depends on the Kapitza length ($\delta = R_k\,\kappa_{bulk}$, where R_k is the thermal boundary resistance). For the pristine np-Si, the parameter F in Eq. (2) can be presented as follows:

$$F = \frac{2 - 2P}{2 + P}.$$

It should be noted, that actual κ_m is lower compared to the thermal conductivity of a bulk material (κ_{bulk}), because of the phonon scattering on a pore's edge. Specifically, when phonon mean free path ($l_{mfp} \sim 300$ nm in bulk silicon[29]) is comparable or bigger than inclusion characteristic size (diameter is less than 5 nm), the thermal conductivity of the matrix reads as follows with respect of Minnich and Chen model[30]:

$$\kappa_m = \frac{\kappa_{bulk}}{1 + \xi \cdot l_{mfp}/4}, \tag{4}$$

Here we use κ_{bulk} which is the thermal conductivity value evaluated by EMD for bulk silicon at room temperature with the S-W potential [31]. l_{mfp} is the phonon mean free path in a bulk material, ξ is the specific surface area of a pore defined as $\xi = A_{por}/V_d$ (A_{por} is the pore surface area, V_d is the volume of simulation box), and it can be considered as an inverse characteristic length.

Since the phonon scattering predefines thermal conductivity reduction at considered scales, we present consolidated dependence of thermal conductivity calculated by molecular dynamics as a function of the specific surface area for both box sizes (see Fig. 2). Additionally, in the inset of the Fig. 2 we depicted the $\kappa_m = \kappa_{MD}(2 + P)/(2 - 2P)$ for pristine np-Si as a function of specific surface area by dots. The solid line corresponds to the fitting of the MD points with Eq. (4). With this fit we estimated that the mean free path (mfp) equals to l_{mfp} = 460±20 nm for bulk silicon, the latter value is in the same order to the one given in the literature (l_{mfp} = 300 nm).
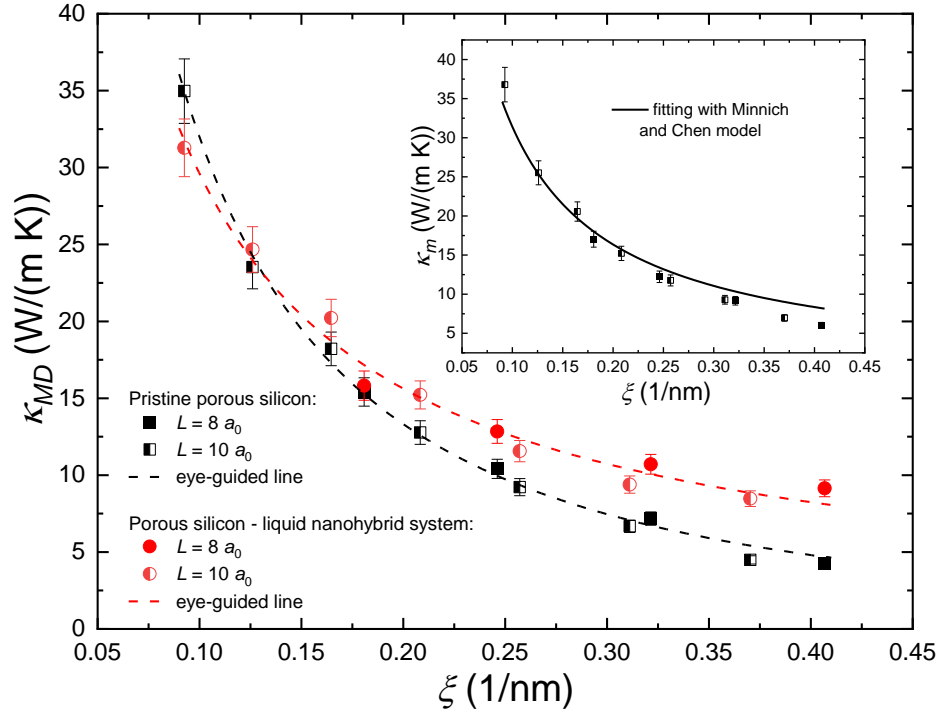
Figure 2. Thermal conductivity of a pristine and a nanocomposite porous silicon as a function of the inverse characteristic length ξ. The results for the dry systems are with black symbols, while for the wet systems with red. Full colors is for the small domain simulations and half colored for the large one. Inset: thermal conductivity normalized by F dry samples, the solid line gives the fitting obtained with Minnich and Chen model[30].

Considering the inset of Fig. 2, it can be noticed that Minnich and Chen model [30] fits MD results well for small inverse characteristic length values (ξ). It should be noted that the model assumes geometrical regime of scattering [32]. It works quite well when the pore radius is much bigger than phonon' wavelength (size parameter $\chi \gg 1$, $\chi = qR$, q is the wavevector). In our case, the mean wavelength is in the same range as a pore radius, therefore the mentioned above model should be modified with the use of Mie scattering theory. As a consequence, when the pore radius increases, the effective medium model does not longer recover the MD results.

In order to take this phenomena into account, one needs to modify the scattering cross sectional area used in the model of Minnich and Chen[30]. In their work, they used an approximate formulation assuming that the cross-sectional area is frequency independent, and it equals to the projected area of a pore ($\sigma_{geom} = n\pi R^2$, n being the number density of scattering centers). However, when wavelength of the phonons is in the same order as a pore diameter, Mie theory[33] gives the following expression for the cross-sectional area:

6

$$\sigma_{Mie} = \sigma_{geom} \times Q_{sca}, \tag{5}$$

Where

$$Q_{sca} = \frac{2}{\chi^2} \sum_{n=1}^{\infty} (2n+1)\left(|a_n|^2 + |b_n|^2\right), \tag{6}$$

$$a_n = \frac{\psi'_n(m\chi)\psi_n(\chi) - m\psi_n(m\chi)\psi'_n(\chi)}{\psi'_n(m\chi)\zeta_n(\chi) - m\psi_n(m\chi)\zeta'_n(\chi)} \tag{7}$$

$$b_n = \frac{m\psi'_n(m\chi)\psi_n(\chi) - \psi_n(m\chi)\psi'_n(\chi)}{m\psi'_n(m\chi)\zeta_n(\chi) - \psi_n(m\chi)\zeta'_n(\chi)}, \tag{8}$$

$m = v_f \rho_f / (v_m \rho_m)$ is the ratio of acoustic impendence of a fluid filler and a matrix (v is sound velocity, ρ is density), $\psi_n(\chi)$ and $\zeta_n(\chi)$ are Riccati-Bessel functions.
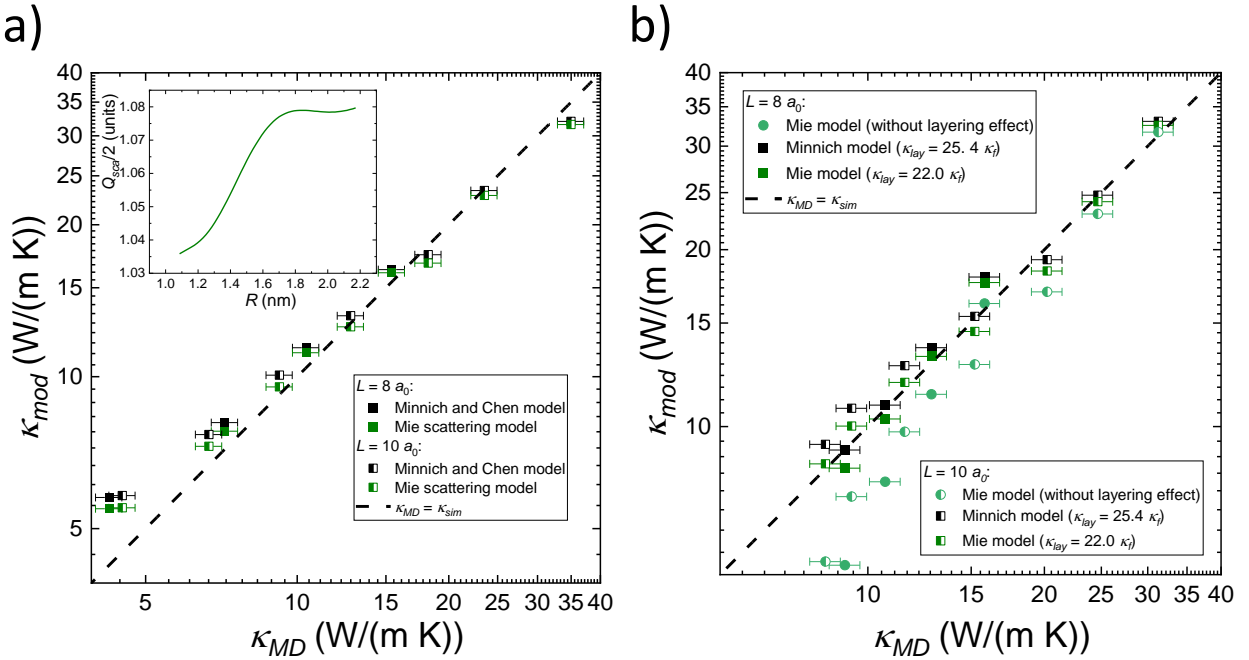

Fig. 3. The diagram presents the correlation between MD and analytical results for pristine porous silicon (a) and for nanohybrid system (b). Filled squares correspond to the simulation domain length equal $8a_0$, half-filled – $10a_0$. Black color represent results obtained based on the Minnich and Chen model, and olive color shows results of Mie scattering model. The inset: Q_{sca} as a function of the pore radius. Squares and circles are devoted to the situations with and without layering effect for the nanohybrid system, respectively.

As a result, equation (Eq.4) can be corrected to take into account Mie scattering dependence. In this framework, matrix thermal conductivity becomes: $\kappa_m = \frac{\kappa_{bulk}}{1 + \delta \cdot \xi \cdot l_{mfp}/4}$,

7

where $2\delta = Q_{sca}$. Fig. 3 presents comparisons between np-Si thermal conductivities obtained with MD simulations and their counterparts derived from the two above discussed effective medium models: Minnich and Chen[30] and Mie scattering. For Mie scattering, we recalculate the mean free path with the use of mean square minimization method to obtain the best fit with our results. We used the following value for both cases l_{mfp} =450±20 nm.

As one can see from the figure, the use of scattering cross-section calculated with the Mie theory gives relatively better correlation with molecular dynamics. This is logical considering Q_{sca} (presented in the inset of Fig. 3a) which exhibits a significant deviation from a constant value in the considered range of pore' radii.

In the Fig. 3b the correlations between the MD simulations and the analytical modeling are plotted. As one can see from the figure, the direct use of Eq. (4) (the data drawn as circles in Fig. 3b) gives significantly underestimated thermal conductivity values while compared to the MD ones. The difference shall arise because of the manifestation of the water layering effect, i.e. the presence of a thin adsorbed layer of liquid with higher density close to solid/liquid interface[34], specifically, the layering effect was observed experimentally[35]. In nanofluids the enhancement of thermal conductivity is also related to this phenomena[36].

The occurrence of a high-density layer close to the interface is revealed by the presence of the water density oscillations (Fig. 4). Density profiles inside a pore were calculated by dividing the space by spherical bins with the centers situated in the middle of the pore (and box). The thickness of the shells was equal to 0.02172 nm. The density in each shell was calculated by averaging of the density during 10 ns. As one can see from the density profiles inside the porous matrix, there is a thin layer of adsorbed liquid with higher density. For evaluation of thickness we used an approach which is based on the equimolar definition of separated surface[37] (see Fig. 4). More specifically, the outer interface was defined as the surface across the radius, which corresponds to half height of the density profile ($(\rho_1 + \rho_2)/2$, where $\rho_1 = 0$ g/cm³ is the density of water outside the sphere and ρ_2 is maximum density). For the inner surface we chose a sphere across the density, which correspond to the average value between density of the second maximum (ρ_3) and minimum (ρ_4). We estimate the thickness of this layer (h) as the thickness of the first two peaks, it was found to be equal 0.5 nm. This values is slightly bigger than those evaluated previously from the Gibbs adsorption (0.4 nm)[38] because of the nature of the curved interface. Computed water density profiles for several pore size are reported in supplementary material.
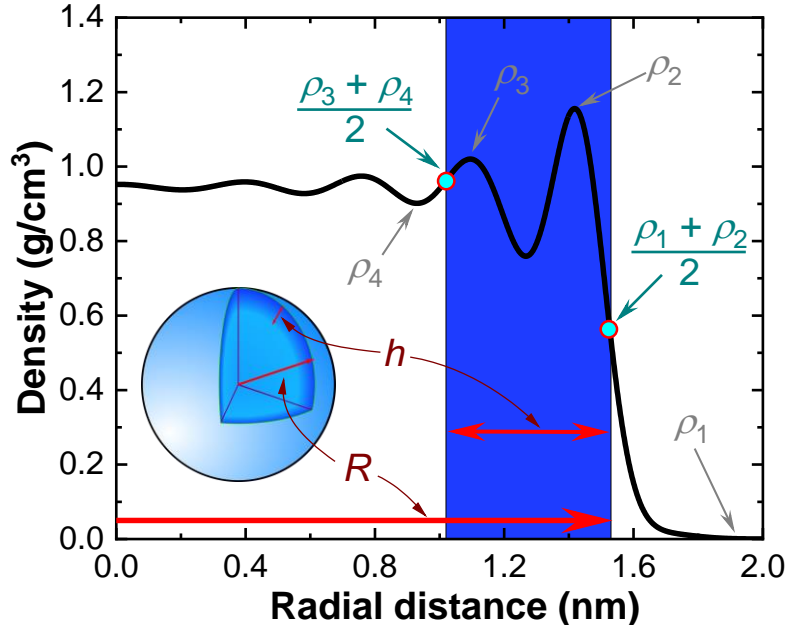
Figure 4. Sketch of the water density profile variations inside a pore. The chosen volume of the adsorbed layer is presented by blue color. The inset demonstrates schematic representation of the structure of a confined water.

To consider the impact of this layer on the system' thermal conductivity, we adopted a model that it is typically used for the estimation of thermal conductivity in nanofluids[36]. In frames of this model thermal conductivity of a liquid (κ_f) in Eq. (3) should be modified as follows

$$\kappa_{f\,mod} = \kappa_f \frac{(2(1-\beta) + (1+\gamma)^3(1+2\beta))\beta}{-(1-\beta) + (1+\gamma)^3(1+2\beta)}, \qquad (9)$$

where $\beta = \kappa_{lay}/\kappa_f$ and $\gamma = h/(R-h)$, κ_{layer} is the thermal conductivity of absorbed layer, and h is it thickness (see Fig. 6).

And the resulting equation for the volume factor is

$$F(P) = \frac{\kappa_{f\,mod} + 2\kappa_{bulk} + 2P(\kappa_{f\,mod} - \kappa_{bulk})}{\kappa_{f\,mod} + 2\kappa_{bulk} - P(\kappa_{f\,mod} - \kappa_{bulk})}. \qquad (10)$$

Here, there is no extra parameter such as interfacial boundary resistance between solid and liquid all the physics is set in absorber layer model.

Squares in Fig.4 corresponds to model values that consider the layer effect (Eq. 10). We vary the value of thermal conductivity of a boundary layer to fit these two sets. As a criterion of the fitting, the minimum of mean least deviation was used. We found the following values of the thermal conductivity of the boundary layer: $\kappa_{lay} = 25.4\kappa_f$ for the Minnich model, $\kappa_{lay} = 22.0\kappa_f$ for the model based on the Mie scattering. This value is higher than the typical value for nanofluids (for example $\kappa_{lay} = 10\kappa_f$ in Yu and

9

Choi[36]). The difference in the sign of the interfacial curvature in the case of a liquid covering nanoparticle (nanofluid) and in the case of a liquid inside porous matrix (nanocomposite) might explain the difference between the nanofluids and the confined water inside a pore. The similar curvature dependence was found by K. Falk et al[39] for the interfacial friction of water at graphitic interfaces with various topologies. They have shown that the friction coefficient exhibits a strong curvature dependence, driving to a fast transport of water in nanometric carbon nanotube membranes. And, the enhanced κ_{lay} in our case compared to the nanofluids might have the same nature as the lower friction coefficient for the negative (for nanopores) or positive (for the nanofluids) curvature.
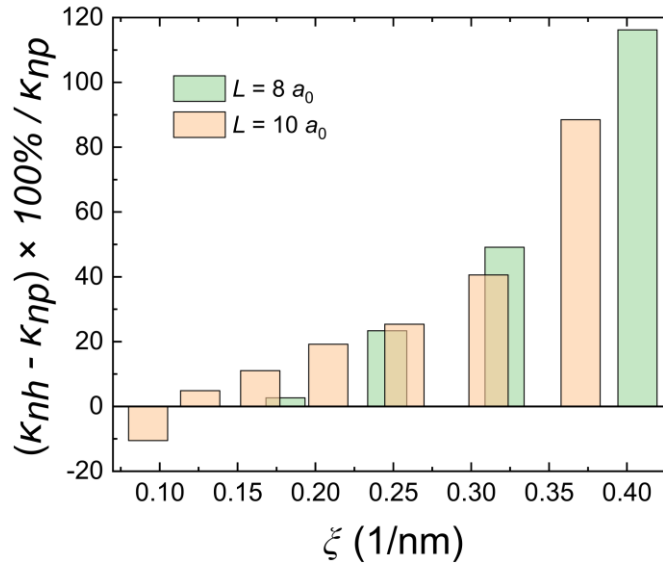

Fig. 5. Thermal conductivity enhancement of thermal conductivity due to nanoconfined water in nanocomposite as a function of specific surface area, κ_{nh} is thermal conductivity of nanohybrid, and κ_{np} is the thermal conductivity of the pristine nanoporous silicon

To summarize, in this work, we considered features of thermal transport in a nano-hybrid composite system with the use of molecular dynamics and analytical modelling. Significant enhancement of the effective thermal conductivity in the nanocomposite system compared to the pristine one was observed (see Fig. 5). This enhancement is getting more pronounced with the increase of the size of the pores. Indeed, thermal conductivity is doubled in nanocomposite system compared to the pristine porous silicon for the biggest considered specific surface area. For the analytical modelling, the approach based on Minnich and Chen model[30] was used. Yet, as considered pore sizes and phonons wavelength were in the same order of magnitude, the above-mentioned approach was modified based on the Mie scattering theory. Furthermore, the development of such methodology was improved to take into account the presence of the surface adsorbed layer of liquid with higher density. It was shown an excellent correlation between the molecular dynamics data and results of analytical modelling. Eventually, the thermal conductivity of the adsorbed layer was estimated to be 25 times greater than in the bulk water. This estimation is based on this correlation and minimization of the MD outputs.

Acknowledgment

References

(1)   Kerner, B. S.; Osipov, V. V. Hot Spots in Semiconductors and Semiconductor Structures. In *Autosolitons*; Springer Netherlands: Dordrecht, 1994; pp 106–109. https://doi.org/10.1007/978-94-017-0825-8_8.

(2)   *Nanostructured Semiconductors: Amorphization and Thermal Properties*; Termentzidis, K., Ed.; Pan Stanford Publishing Pte. Ltd.: Singapore, 2017.

(3)   Ali, N.; Teixeira, J. A.; Addali, A. A Review on Nanofluids: Fabrication, Stability, and Thermophysical Properties. *J. Nanomater.* **2018**, *2018*. https://doi.org/10.1155/2018/6978130.

(4)   Pastoriza-Gallego, M. J.; Casanova, C.; Páramo, R.; Barbés, B.; Legido, J. L.; Piñeiro, M. M. A Study on Stability and Thermophysical Properties (Density and Viscosity) of Al2O3 in Water Nanofluid. *J. Appl. Phys.* **2009**, *106* (6), 064301. https://doi.org/10.1063/1.3187732.

(5)   Holkar, C. R.; Jain, S. S.; Jadhav, A. J.; Pinjari, D. V. Scale-Up Technologies for Advanced Nanomaterials for Green Energy. In *Nanomaterials for Green Energy*; Elsevier, 2018; pp 433–455. https://doi.org/10.1016/B978-0-12-813731-4.00014-X.

(6)   Bhanvase, B. A.; Barai, D. P.; Sonawane, S. H.; Kumar, N.; Sonawane, S. S. Intensified Heat Transfer Rate With the Use of Nanofluids. In *Handbook of Nanomaterials for Industrial Applications*; Elsevier, 2018; pp 739–750. https://doi.org/10.1016/B978-0-12-813351-4.00042-0.

(7)   Gomès, S.; David, L.; Lysenko, V.; Descamps, a; Nychyporuk, T.; Raynaud, M. Application of Scanning Thermal Microscopy for Thermal Conductivity Measurements on Meso-Porous Silicon Thin Films. *J. Phys. D. Appl. Phys.* **2007**, *40* (21), 6677–6683. https://doi.org/10.1088/0022-3727/40/21/029.

(8)   Dubyk, K.; Chepela, L.; Lishchuk, P.; Belarouci, A.; Lacroix, D.; Isaiev, M. Features of Photothermal Transformation in Porous Silicon Based Multilayered Structures. *Appl. Phys. Lett.* **2019**, *115* (2), 021902. https://doi.org/10.1063/1.5099010.

(9)   Tang, G. H.; Zhao, Y.; Zhai, G. X.; Bi, C. Phonon Boundary Scattering Effect on Thermal Conductivity of Thin Films. *J. Appl. Phys.* **2011**, *110* (4), 046102. https://doi.org/10.1063/1.3622317.

(10) Verdier, M.; Lacroix, D.; Didenko, S.; Robillard, J.-F.; Lampin, E.; Bah, T.-M.; Termentzidis, K. Influence of Amorphous Layers on the Thermal Conductivity of Phononic Crystals. *Phys. Rev. B* **2018**, *97* (11), 115435. https://doi.org/10.1103/PhysRevB.97.115435.

(11) Verdier, M.; Lacroix, D.; Termentzidis, K. Thermal Transport in Two- and Three-Dimensional Nanowire Networks. *Phys. Rev. B* **2018**, *98* (15), 155434. https://doi.org/10.1103/PhysRevB.98.155434.

(12) Verdier, M.; Termentzidis, K.; Lacroix, D. Crystalline-Amorphous Silicon Nano-Composites: Nano-Pores and Nano-Inclusions Impact on the Thermal Conductivity. *J. Appl. Phys.* **2016**, *119* (17), 175104. https://doi.org/10.1063/1.4948337.

(13) Andrusenko, D.; Isaiev, M.; Tytarenko, a.; Lysenko, V.; Burbelo, R. Size Evaluation of the Fine Morphological Features of Porous Nanostructures from the Perturbation of Heat Transfer by a Pore Filling Agent. *Microporous Mesoporous Mater.* **2014**, *194*, 79–82. https://doi.org/10.1016/j.micromeso.2014.03.045.

(14) Lishchuk, P.; Andrusenko, D.; Isaiev, M.; Lysenko, V.; Burbelo, R. Investigation of Thermal Transport Properties of Porous Silicon by Photoacoustic Technique. *Int. J. Thermophys.* **2015**, *36* (9), 2428–2433. https://doi.org/10.1007/s10765-015-1849-8.

(15) Thomas, J. A.; Iutzi, R. M.; McGaughey, A. J. H. Thermal Conductivity and Phonon Transport in Empty and Water-Filled Carbon Nanotubes. *Phys. Rev. B - Condens. Matter Mater. Phys.* **2010**, *81* (4), 1–7. https://doi.org/10.1103/PhysRevB.81.045413.

(16) Barisik, M.; Beskok, A. Temperature Dependence of Thermal Resistance at the Water/Silicon Interface. *Int. J. Therm. Sci.* **2014**, *77*, 47–54. https://doi.org/10.1016/j.ijthermalsci.2013.10.012.

(17) Pham, A. T.; Barisik, M.; Kim, B. Molecular Dynamics Simulations of Kapitza Length for Argon-Silicon and Water-Silicon Interfaces. *Int. J. Precis. Eng. Manuf.* **2014**, *15* (2), 323–329. https://doi.org/10.1007/s12541-014-0341-x.

(18) Khare, R.; Keblinski, P.; Yethiraj, A. Molecular Dynamics Simulations of Heat and Momentum Transfer at a Solid-Fluid Interface: Relationship between Thermal and Velocity Slip. *Int. J. Heat Mass Transf.* **2006**, *49* (19–20), 3401–3407. https://doi.org/10.1016/j.ijheatmasstransfer.2006.03.005.

(19) Chakraborty, S.; Kumar, H.; Dasgupta, C.; Maiti, P. K. Confined Water: Structure, Dynamics, and Thermodynamics. *Acc. Chem. Res.* **2017**, *50* (9), 2139–2146. https://doi.org/10.1021/acs.accounts.6b00617.

(20) Hu, M.; Goicochea, J. V.; Michel, B.; Poulikakos, D. Water Nanoconfinement Induced Thermal Enhancement at Hydrophilic Quartz Interfaces. *Nano Lett.* **2010**, *10* (1), 279–285. https://doi.org/10.1021/nl9034658.

(21) Watanabe, K.; Tadokoto, M.; Oguni, M. Thermal Characteristics of Channel Water Confined in Nanopores with Crystalline Pore-Wall Structure in [M(H 2 Bim) 3](TMA)· n H 2 O. *J. Phys. Chem. C* **2012**, *116* (21), 11768–11775. https://doi.org/10.1021/jp302222r.

(22) Stillinger, F. H.; Weber, T. a. Computer Simulation of Local Order in Condensed Phases of Silicon.

Phys. Rev. B **1985**, *31* (8), 5262–5271. https://doi.org/10.1103/PhysRevB.31.5262.

(23) Berendsen, H. J. C.; Grigera, J. R.; Straatsma, T. P. The Missing Term in Effective Pair Potentials. *J. Phys. Chem.* **1987**, *91* (24), 6269–6271. https://doi.org/10.1021/j100308a038.

(24) Isaiev, M.; Burian, S.; Bulavin, L.; Gradeck, M.; Lemoine, F.; Termentzidis, K. Efficient Tuning of Potential Parameters for Liquid–Solid Interactions. *Mol. Simul.* **2016**, *42* (11), 910–915. https://doi.org/10.1080/08927022.2015.1105372.

(25) Plimpton, S. Fast Parallel Algorithms for Short-Range Molecular Dynamics. *J. Comput. Phys.* **1995**, *117* (1), 1–19. https://doi.org/10.1006/jcph.1995.1039.

(26) Abad, B.; Borca-Tasciuc, D. A.; Martin-Gonzalez, M. S. Non-Contact Methods for Thermal Properties Measurement. *Renew. Sustain. Energy Rev.* **2017**, *76* (March), 1348–1370. https://doi.org/10.1016/j.rser.2017.03.027.

(27) Nan, C. W.; Birringer, R.; Clarke, D. R.; Gleiter, H. Effective Thermal Conductivity of Particulate Composites with Interfacial Thermal Resistance. *J. Appl. Phys.* **1997**, *81* (10), 6692–6699. https://doi.org/10.1063/1.365209.

(28) Maxwell, J. C. *Electricity and Magnetism*; Clarendon Press: Oxford, UK, 1873.

(29) Ju, Y. S.; Goodson, K. E. Phonon Scattering in Silicon Films with Thickness of Order 100 Nm. *Appl. Phys. Lett.* **1999**, *74* (20), 3005–3007. https://doi.org/10.1063/1.123994.

(30) Minnich, A.; Chen, G. Modified Effective Medium Formulation for the Thermal Conductivity of Nanocomposites. *Appl. Phys. Lett.* **2007**, *91* (7), 073105. https://doi.org/10.1063/1.2771040.

(31) Kuryliuk, V.; Nepochatyi, O.; Chantrenne, P.; Lacroix, D.; Isaiev, M. Thermal Conductivity of Strained Silicon: Molecular Dynamics Insight and Kinetic Theory Approach. *J. Appl. Phys.* **2019**, *126* (5), 055109. https://doi.org/10.1063/1.5108780.

(32) Wu, D.; Petersen, A. S.; Poon, S. J. Effective Scattering Cross-Section in Lattice Thermal Conductivity Calculation with Differential Effective Medium Method. *AIP Adv.* **2013**, *3* (8). https://doi.org/10.1063/1.4818972.

(33) Jan-Patrick Schäfer. Implementierung Und Anwendung Analytischer Und Numerischer Verfahren Zur Lösung Der Maxwellgleichungen Für Die Untersuchung Der Lichtausbreitung in Biologischem Gewebe, 2011. https://doi.org/10.18725/OPARU-1914.

(34) Iarlori, S.; Carnevali, P.; Ercolessi, F.; Tosatti, E. Structure and Correlations of a Liquid Metal Surface: Gold. *Surf. Sci.* **1989**, *211–212*, 55–60. https://doi.org/10.1016/0039-6028(89)90753-X.

(35) Paineau, E.; Albouy, P.-A.; Rouzière, S.; Orecchini, A.; Rols, S.; Launois, P. X-Ray Scattering Determination of the Structure of Water during Carbon Nanotube Filling. *Nano Lett.* **2013**, *13* (4), 1751–1756. https://doi.org/10.1021/nl400331p.

(36) Yu, W.; Choi, S. U. S. The Role of Interfacial Layers in the Enhanced Thermal Conductivity of Nanofluids : A Renovated Maxwell Model. *J. Nanoparticle Res.* **2003**, *5*, 167–171.

(37) Burian, S.; Isaiev, M.; Termentzidis, K.; Sysoev, V.; Bulavin, L. Size Dependence of the Surface

Tension of a Free Surface of an Isotropic Fluid. *Phys. Rev. E* **2017**, *95* (6), 062801(1-5). https://doi.org/10.1103/PhysRevE.95.062801.

(38) Isaiev, M.; Burian, S.; Bulavin, L.; Chaze, W.; Gradeck, M.; Castanet, G.; Merabia, S.; Keblinski, P.; Termentzidis, K. Gibbs Adsorption Impact on a Nanodroplet Shape: Modification of Young–Laplace Equation. *J. Phys. Chem. B* **2018**, *122* (12), 3176–3183. https://doi.org/10.1021/acs.jpcb.7b12358.

(39) Falk, K.; Sedlmeier, F.; Joly, L.; Netz, R. R.; Bocquet, L. Molecular Origin of Fast Water Transport in Carbon Nanotube Membranes: Superlubricity versus Curvature Dependent Friction. *Nano Lett.* **2010**, *10* (10), 4067–4073. https://doi.org/10.1021/nl1021046.

Supplementary material.

S1 Density profile inside pores.

The dependence of the water density (ρ) on the radial distance from the pore' center (r) for different pore radii (R). As one can see, for different pore' radius, the density profile has the same structure with the presence of well-define maximum peak and further oscillations. The width of interfacial area is almost the same for all radii as it is depicted in the inset of the figure, where the density profiles are shifted by $r_{\rho_{max}/2}$ to align them to the solid/liquid interface, where the water density is equal to the half density of the first peak ($\rho_{max}/2$).
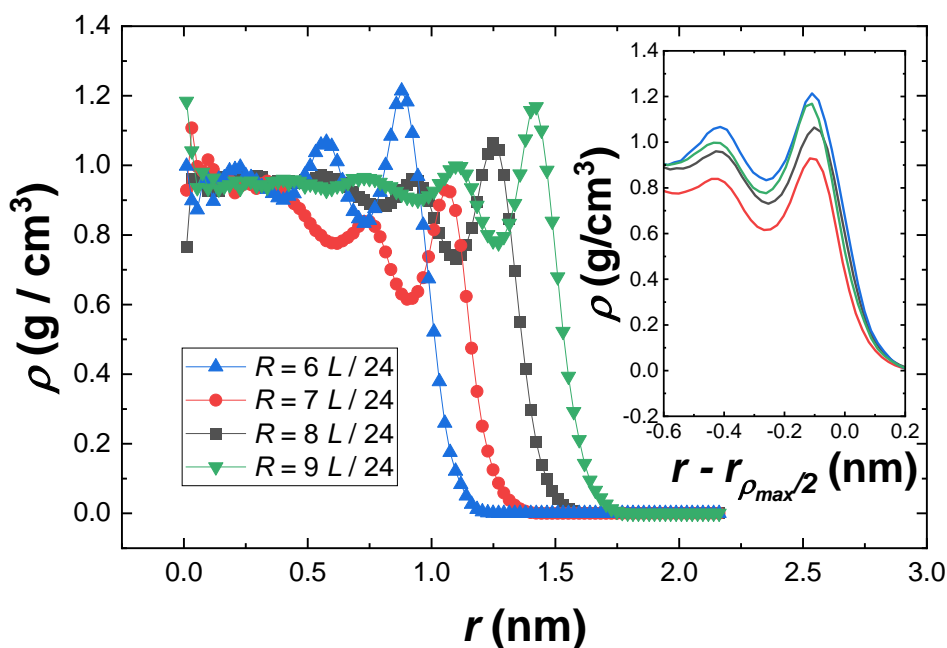

Fig. S1. Density distribution of water inside a pore for different pore' radii. The inset presents the same density profiles but with a focus close to the interface and shifted on R.